AGU PUBLICATIONS

Water Resources Research

RESEARCH ARTICLE
10.1002/2017WR020797

Space-Time Patterns of Meteorological Drought Events in the European Greater Alpine Region Over the Past 210 Years

K. Haslinger[1,2] and G. Blöschl[2]

[1]Climate Research Department, Central Institute for Meteorology and Geodynamics, Vienna, Austria, [2]Institute for Hydraulic and Water Resources Engineering, and Centre for Water Resource Systems, Vienna University of Technology, Vienna, Austria

Key Points:
- A new method is proposed for detecting atmospheric drought events in terms of their frequency, duration, intensity, and severity
- Multidecadal variations of drought frequency, duration, intensity, and severity over the past 210 years exist in the GAR, but no trends
- Most severe events center either around the Northwest or the Southeast of the GAR

Correspondence to:
K. Haslinger,
klaus.haslinger@zamg.ac.at

Citation:
Haslinger, K., & Blöschl, G. (2017). Space-time patterns of meteorological drought events in the European Greater Alpine Region over the past 210 years. *Water Resources Research*, *53*, 9807–9823. https://doi.org/10.1002/2017WR020797

Received 20 MAR 2017
Accepted 30 OCT 2017
Accepted article online 15 NOV 2017
Published online 28 NOV 2017

Abstract Droughts may have tremendous impacts on humans. However, the space-time characteristics of droughts are not very well understood, as case studies usually focus on individual drought events. Here we investigate the spatiotemporal drought characteristics of a large sample of events over the past 210 years in the Greater Alpine Region of Central Europe. We use monthly precipitation data, and flag, for each grid point, time steps with precipitation below a 20% percentile. We then propose a new method that detects drought events by connecting the flagged elements to space-time drought regions. In contrast to the traditional drought indices that are based on a fixed, prescribed time window, this method is able to identify droughts of different durations in an objective way. The data show multidecadal variations of drought frequency, duration, intensity, and severity, but no consistent trends over the 210 year period. The top 5% of events in terms of their severity show a shift in seasonality from winter/spring events in the late nineteenth century toward autumn events during the last decades of the twentieth century. The most severe events center either in the Northwest or in the Southeast of the region analyzed. We found no significant correlations of drought frequency, duration, intensity, and severity with the temperature increases in the past three decades. Dry springs significantly enhance temperatures during summer droughts, suggesting a soil moisture-temperature feedback.

1. Introduction

Droughts are natural hazards with the potential to cause immense damage to agriculture, water supply, and energy production, and they can severely affect ecosystems (Vincente-Serrano et al., 2012). The European summer drought of 2003 (García-Herrera et al., 2010) caused economical losses of around €15 billion (UNEP, 2006). The 2015 drought (van Lanen et al., 2016) and a series of winter droughts in the United Kingdom from 2010 to 2012 (Kendon et al., 2013) had similarly negative effects.

However, the understanding of long-term drought variability has been hampered by the relatively short time periods analyzed. Studies usually focus on individual events and/or records of 100 years or less. The SREX report (IPCC, 2012) stated that drought trends in Central Europe are either inconsistent or statistically insignificant and that there is low confidence in the attribution of changes in droughts at the level of individual regions. Gaining knowledge on past drought behavior in Europe over a longer period is therefore of utmost importance (Mishra & Singh, 2010).

Several global to continental scale analyses of past drought trends have been performed. Using various variants of the Palmer Drought Severity Index (PDSI; Palmer, 1965), Dai (2011) found trends toward dryer conditions over Southern Europe, with an increasing trend during recent decades, which they attributed to increasing evapotranspiration associated with increasing air temperatures. These results are not fully consistent with soil moisture trends from simulations by the VIC model (Sheffield & Wood, 2008), which showed no significant changes in soil moisture over the 1950–2000 period (Northern Europe $+0.096\%\ yr^{-1}$, Southern Europe $-0.048\%\ yr^{-1}$). Using the self-calibrating Palmer Drought Severity Index (scPDSI; Wells et al., 2004), van der Schrier et al. (2013) found an increase in the percentage area under moderately dry conditions in the Mediterranean and a trend toward wetter conditions in the North of Europe, although these trends were not significant.

More specific analyses focusing on Europe were carried out by Lloyd-Hughes and Saunders (2002) who found an increasing frequency of extreme droughts in continental Eastern Europe during the twentieth

century period, based on the PDSI, and similar results when considering the SPI on a 12 month accumulation time scale. The most extreme droughts in Europe from 1950 to 2012 where analyzed by Spinoni et al. (2015) based on a combined indicator that takes precipitation and evapotranspiration into account, considering 3 and 12 month accumulation time scales over predefined European subregions. They concluded that the 1950s were the time period with exceptionally long, widespread, and intense droughts and that Western and Southern Europe showed highest drought frequency and severity in the past two decades.

A joint assessment of precipitation and temperature quantiles of nine stations across Europe (Beniston, 2009) showed a significant increase in warm-dry conditions from 1901 to 2009, exceeding the overall warming in Europe. The author argues that this might be related to soil moisture-temperature feedbacks (Seneviratne et al., 2006). van der Schrier et al. (2006) detected negative trends of the scPDSI, indicating dryer summer conditions in Europe until the 1990s with a decline afterward, which is not fully consistent with the results of Dai et al. (2004). van der Schrier et al. (2006) conducted a regionalization based on Empirical Orthogonal Teleconnections (Van den Dool et al., 2000) and found persistent dry summers in the Balkans from 1983 to 1994 and from the beginning of the 2000s, only minor changes in Northwestern Europe and very dry conditions in the 1940s in Southern France/Northern Italy. In another study, van der Schrier et al. (2007) analyzed droughts in the Greater Alpine Region (GAR) of Central Europe from 1801 to 2003, using spatially averaged time series of the scPDSI based on predefined subregions (Auer et al., 2007). They found that the 1850–1870s and 1940–1950s were exceptionally dry, however, long-term trends were not significant.

Drought is a phenomenon that emerges in space *and* time and can be characterized by attributes such as duration, spatial extent, and intensity (Sheffield & Wood, 2007). Yet many studies, choose regions a priori and analyze (one-dimensional) time series of regional averages of various drought variables (precipitation, drought indices, streamflow, etc.), even though these regions may not be tailored to drought analyses (e.g., Dai, 2011; Sheffield & Wood, 2008; Spinoni et al., 2015; van der Schrier et al., 2007). On the other hand, there are studies investigating the spatial structure (a two-dimensional assessment) of drought patterns (e.g., Patel et al., 2007; Vincente-Serrano, 2006) but most of them utilize drought indicators on fixed accumulation time scales (moving averaging time windows). Neither of these two groups of studies considers droughts as a (three-dimensional) space-time phenomenon.

One method that does consider space and time jointly is the Severity-Area-Duration (SAD) method of Andreadis et al. (2005) that evaluates soil moisture and runoff as a function of prescribed areas and prescribed durations (Andreadis et al., 2005; Samaniego et al., 2013; Sheffield et al., 2009; Zhai et al., 2017). Its focus on the areal extent may mask the temporal evolution of droughts which prompted Lloyd-Hughes (2012) to evaluate the space-time structure and similarity of droughts. However, this method is less well suited for analyzing the general characteristics of droughts and their long-term evolution in a region.

This paper proposes a new method for detecting atmospheric drought events that fully accounts of the dynamic space-time behavior of droughts. We use the method to analyze precipitation data in the Greater Alpine Region (GAR) over the past 210 years to detect space-time drought events. Specifically, the aims of the paper are (i) to develop a new method of space-time drought event detection, (ii) to analyze the temporal evolution of drought event characteristics (duration, intensity, and severity) in the GAR over the past 210 years, (iii) to analyze the spatial patterns of droughts as a function of severity and duration, and (iv) to investigate the influence of recent air temperature increases on the three main drought characteristics.

We are interested in meteorological drought events in Central Europe, considering precipitation deficit as the variable of interest. Our region of interest is the European Greater Alpine Region (Auer et al., 2007). Although it is only part of Europe, it covers three main climate divisions in Europe (Mediterranean, temperate oceanic and continental climates) and the three main spatial modes of drought identified by van der Schrier et al., (2006) in the Balkans, Eastern France/Southern Germany, and Southern France/Northern Italy, respectively.

2. Data

We use gridded data of monthly precipitation totals covering the area from 4° to 19° East and 43° to 49° North, known as the Greater Alpine Region (GAR, Figure 1). This data set was created by Efthymiadis et al.

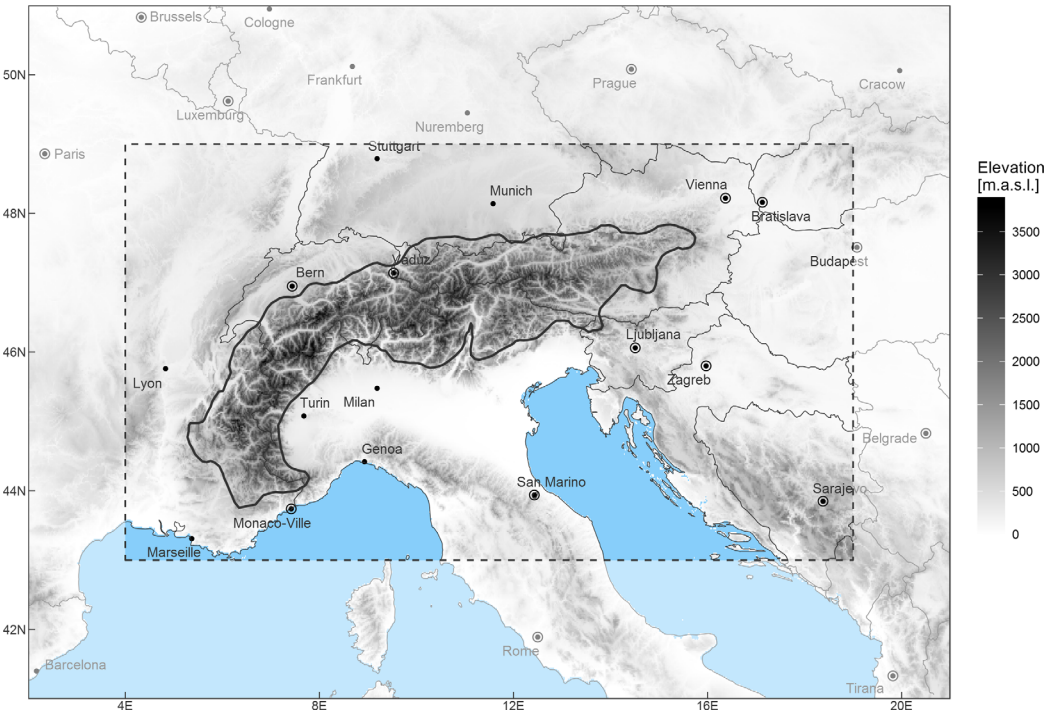

Figure 1. Study domain and orography. The dashed box indicates the Greater Alpine Region (GAR) which is the area of interest. For reference the generalized 1,000 m asl elevation contour is shown as a solid black line.

(2006) in the frame of the HISTALP activities (Auer et al., 2007). HISTALP is a database covering the GAR containing long-term (from 1760), high quality, homogenized station time series of various climate variables such as air temperature, air pressure, sunshine duration, and precipitation as well as gridded products of air temperature, solid, and liquid precipitation. The data set of Efthymiadis et al. (2006) has a spatial resolution of 10 arc min (∼16 km) and covers the time period from 1801 to 2010. The original data set ended 2003 and was updated for the purposes of this paper. Auer et al. (2007) homogenized the station data the gridded data set is based on and conducted a comprehensive quality check. Efthymiadis et al. (2006) performed a skill assessment of the gridding process and showed that the skill increases during the first decades of the nineteenth century and reaches a plateau around 1850. The remaining uncertainties in the gridding process during the first decades of the nineteenth century have to be kept in mind when interpreting the results of this paper.

Droughts are considered from different perspectives across disciplines. In this study, we focus on meteorological droughts, defined as below average precipitation totals. In a humid climate such as the GAR, precipitation deficit is the main driver for drought development, altered by enhanced evapotranspiration (e.g., Burke & Brown, 2008). We therefore consider precipitation a meaningful variable for analyzing the space-time variability of droughts.

Gridded monthly mean temperature data of the GAR (Chimani et al., 2013) are used as well. They have a spatial resolution of 5 arc min (∼8 km), and cover the period from 1780 to 2014.

3. Methods

In contrast to the traditional drought indices, such as the SPI, that are based on a fixed, prescribed accumulation time windows and a fixed region, we propose a new method that detects drought events by connecting space-time elements to a coherent space-time drought region. Although widely used, the SPI has some limitations, particularly in terms of a severity assessment of extremes at the tails of the distribution (Naresh Kumar et al., 2009). Stagge et al. (2015) also highlight the uncertainties associated with the distribution fitting at the tails. This uncertainty would translate into the SPI estimates of the most extreme quantiles thus making the severity assessment noisy, particularly if adjacent pixels are compared. For example, the most

extreme value at the dry side of the distribution might be −4 at one grid point, but may be −5 at the neighboring one. Both show their most extreme quantile values close to zero, but the SPI itself would be different, simply due to distribution-fitting uncertainty. The use of quantiles instead of the SPI has the advantage of having a fixed lower boundary for the most extreme values, which allows us to identify droughts of different durations in a more robust way. The proposed method consists of four steps.

In a first step, we calculate moving averages of monthly precipitation data over a 3 month time window (centered on the actual month) on every grid point in the domain. This smoothing of the precipitation data is necessary to retrieve meaningful space-time structures of droughts. Alternatively using monthly precipitation totals, for example, would cause interruptions of events along the time axis. A Gamma distribution is fitted to the averaged precipitation, separately for every month of the year and every grid point, in a similar way as in the Standardized Precipitation Index (SPI; McKee et al., 1993). The choice of the Gamma distribution is based on Stagge et al. (2015) who found that it provides better fits to precipitation data in Europe than alternative distributions. To separate dry from nondry areas, we chose the 0.2 quantile as a threshold. Although this value is not very extreme (equivalent to a 5 year return period, and an SPI-value of −0.84), it is commonly used to identify dry precipitation anomalies, for example, in the U.S. drought monitor (Svoboda et al., 2002). For a more intuitive assessment of drought intensity, these quantiles are scaled in order to get higher values with higher drought intensity using equation (1):

$$q_{\text{int}} = (\xi - p)/\xi, \tag{1}$$

where q_{int} is the quantile drought intensity, p is the probability of nonexceedance, and ξ is the threshold of the quantile of 0.2. The intensity measure q_{int} ranges between −4 (probability of nonexceedance of 1) representing wettest conditions and 1 (probability of nonexceedance of 0) representing the most severe drought of a particular location and month. Step 2 deals with the spatial component of the detection algorithm, where *contiguous* areas with drought intensity values q_{int} larger than 0 are identified. We use an algorithm starting from the first grid point with positive drought intensity detected in the field, searching for neighboring grid points with dry conditions ($q_{\text{int}} > 0$, grid points joining only diagonally at their corners are not considered). Once a contiguous drought area (DA) is detected, the field is further scanned for dry condition areas until all grid points are checked. The result is a table with all individual drought areas, their time of occurrence (year and month), and location of every grid point and their intensity value q_{int}.

Step 3 focuses on the temporal component of the detection algorithm. Identified drought areas are compared with the drought areas of the subsequent time step. If these areas do overlap, they are considered to belong to the same drought event (DE), an entity in both space and time. However, we apply three criteria that have to be met for a space-time region to be considered a drought event: (i) single drought areas must be larger than 10% (∼77,000 km^2) of the GAR; we decided for this criterion in order to ensure that only areas with a reasonable size and therefore impact are considered as drought event candidates; (ii) the overlap of the areas must be at least 50% of the smaller area; and (iii) the smaller area must be at least 25% of the larger area. These criteria were identified on the basis of test runs, comparing the detected events with those from the literature. Figure 2 shows three hypothetical cases of three subsequent time steps with overlapping drought areas (DAs) (top) and the outcome of the criterion assessment (bottom). In case 1, all criterions are met, yielding an event consisting of all three DAs. In case 2, the overlap criterion is violated for areas A2 and A3, which results in two separate events, the first one including DAs A1 and A2 and the second including A3. In case 3, all three criterions are violated. The size criterion is violated by A3, the other two DAs (A1 and A2) are big enough, but their overlap is too small. Consequently A1 and A2 are assumed to be separate events and A3 is not considered at all.

Figure 3 shows a real event identified from December 1862 to March 1863. The DAs of subsequent months overlap with each other according to the three criteria given above.

The last step consists of evaluating the drought characteristics. One important part is the assessment of the drought event severity. We assume that an event is more severe if (i) the quantile drought intensity q_{int} is large, (ii) the area under drought is large, and (iii) the duration of the drought is large. The first two components are combined into an intensity measure for every time step over the drought duration:

$$I = \sum_{i=1}^{n} q_{\text{int}}, \quad i \in DA \tag{2}$$

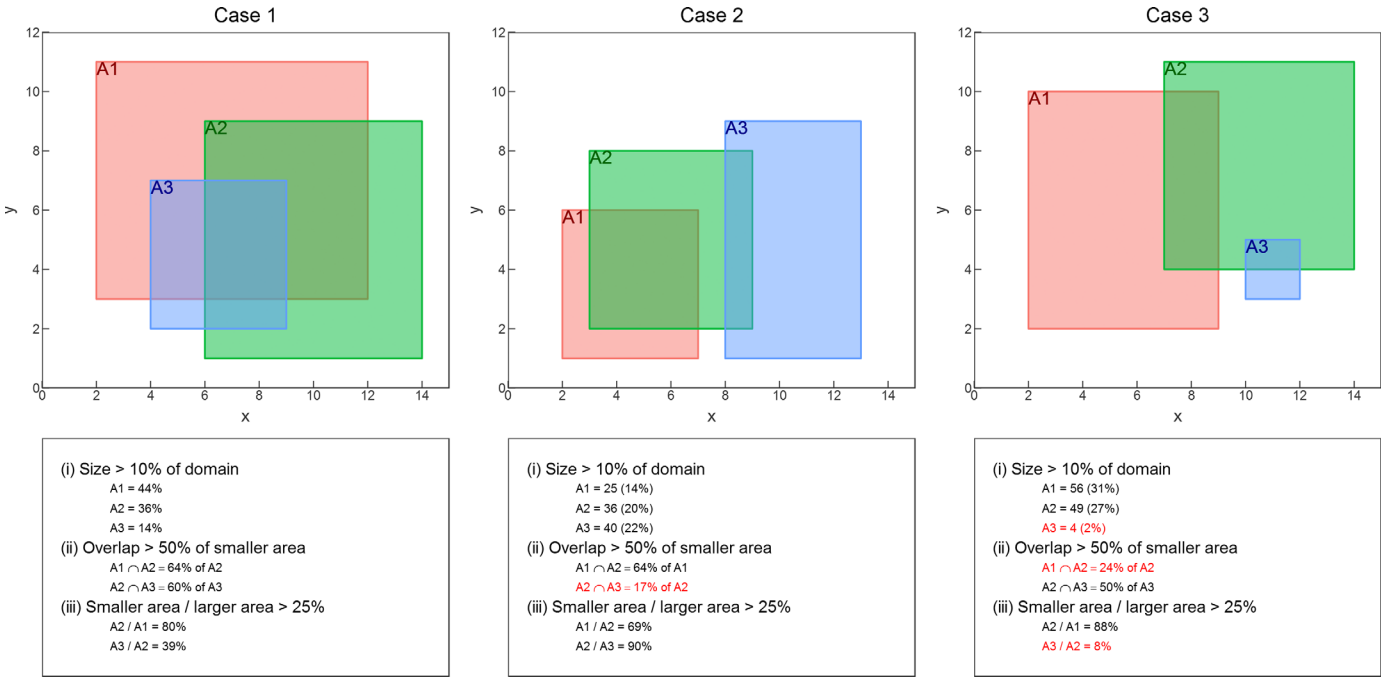

Figure 2. Schematics of three cases of drought event detection; (top) idealized drought areas as rectangles (A1–A3) within a region of 15 × 12 length units; (bottom) check of the three criterions (i–iii) that have to be met if the areas are to be joined (see text for details); criterion violations are indicated by red font.

where I is the intensity, n is the number of grid points i within the drought area (DA), and q_{int} is the quantile drought intensity. Consequently I increases with both the number of drought grid points and their quantile drought intensity. Figure 4a shows the temporal evolution of the intensity from the example in Figure 3. From the onset of the drought in December 1862, intensity is around 150 with no large variation until February. As can be seen, the intensity depends on the grid size of the utilized data set, so it has to be assessed in relation to the whole grid. One could also use the area of the grid which would introduce units of km^2, but this would overemphasize the spatial component, although the threshold deviation (q_{int}, dimensionless) is equally important. So in the case of December 1862, we have $I = 150$ which could either be an area of 150 grid points (~38,000 km^2) all in most extreme drought conditions ($q_{int} = 1$) or 300 grid point (~76,000 km^2) with $q_{int} = 0.5$. In our case, $q_{int} = 0.3$ and the number of grid points is 492. Comparing this evolution with Figures 3a–3c, the areas under drought of the first two time steps are similar in size and in terms of q_{int}. However, in February q_{int} is larger, but the area is smaller, resulting in rather similar intensity values. The peak of the drought intensity was reached in March 1863 with an intensity in excess of 400, which is a consequence of the large area and the large values of q_{int} (Figure 3d). Finally, we calculate the overall drought severity as

$$S = \sum_{i=1}^{n} I_{i \in DE}, \tag{3}$$

where S is the severity, which is the sum of all intensities I within the same drought event, and n is the number of time steps comprising the drought event. Consequently, summing up areas in terms of grid points

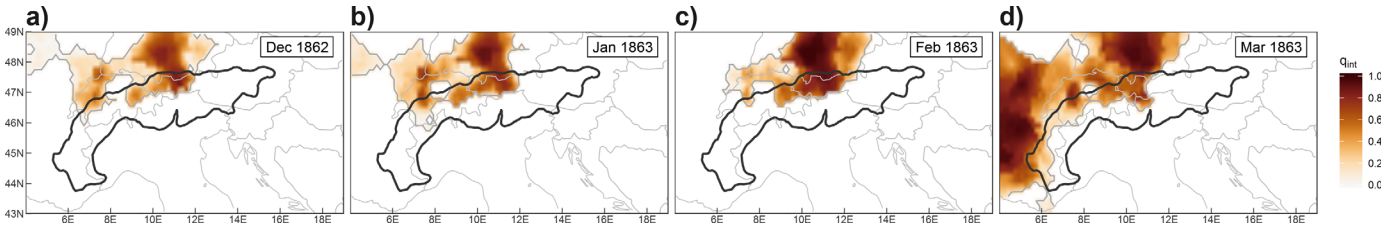

Figure 3. Example of a detected meteorological drought event in space and time. The event is identified from (a) January 1863 to (d) April 1863. The grey lines mark zero contour lines of the quantile drought intensities (q_{int}). The colors refer to the quantile drought intensities, darker colors referring to drier areas (larger q_{int}).

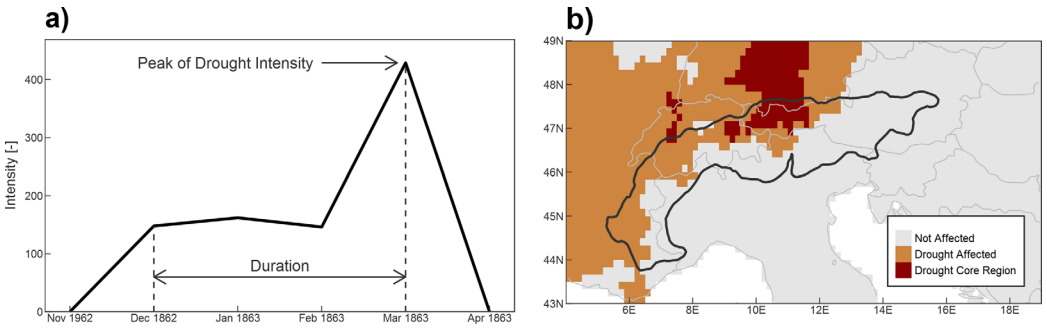

Figure 4. Temporal evolution of a drought event (referring to Figure 3): the thick black line represents the drought intensity, bounded by the start (December 1862) and the end (March 1863), indicating (a) a duration of 4 months, and the drought intensity peaking in March 1863; (b) representation of three different spatial entities during the event: areas not affected by drought, areas affected by drought and the drought core region.

has the same implications as mentioned above considering the intensity assessment, meaning that the interpretation of S is dependent on the grid resolution. For the further analysis the following event characteristics are used: severity, the monthly intensity as well as the mean intensity (severity divided by duration) and duration.

In addition to the temporal evolution of droughts, we are interested in their spatial characteristics. As illustrated by the example in Figure 3, one time step may contribute disproportionally to the overall drought affected area of an event. It may therefore not be useful to consider the overall drought affected area in a spatial analysis. Instead, we defined drought core regions (DCRs) as shown in Figure 4b. Grey areas denote regions not affected by the drought, brown areas the overall extent of the drought (see Figure 3) and red areas the drought core region. We define a DCR as those grid points of an identified event with a time-average q_{int} of at least 0.5, which represents a quantile value of 0.1 or an SPI of -1.29. This choice is based on the assumption that the area most affected by the drought has to have a sustained signal of drought during the whole event with a high value of q_{int}. A comparison of Figures 3 and 4b illustrates that the DCR comprises those areas with the most sustained and intense drought signal during the drought event.

One further aspect, we considered is the temperature anomaly during an event. Similarly to precipitation, we calculated 3 month moving temperature averages. From these, anomalies were calculated for each month individually, with respect to the long-term (1801–2008) mean. Intersecting these temperature anomaly grids with the detected areas of the drought events, we obtained the temperature anomalies corresponding to the identified drought areas.

4. Results

4.1. Temporal Evolution of Drought Characteristics

A total of 663 drought events were detected in the time period from 1801 to 2010. Thirty year averages of the three main attributes of all drought events (duration, severity, and mean intensity) as well as 30 year frequencies are displayed in Figure 5a. Frequency shows a continuous increase from the beginning of the data set with a first peak around the 1880s and a second, more pronounced one, around the 1940s with 120 events per 30 years followed by a decrease to around 80 events per 30 years. Duration shows a similar increase until the mid-nineteenth century toward to 3 months, a secondary minimum in the 1930s, and a slight increase during the rest of the twentieth century. Severity shows the most prominent peak in the middle of the nineteenth century with mean values up to 1,400. During the twentieth century, severity varies around 1,000. The mean intensity shows even stronger fluctuations with a prominent peak of 370 around the 1860s, very similar to the peak in severity. A sharp decrease follows reaching a minimum of around 270 at the beginning of the twentieth century. There is a secondary maximum around the 1940s, and a secondary minimum around the 1970s.

If one analyses only the top 5% of the events in terms of their severity (34 drought events) a somewhat different time evolution of the event characteristics emerges (Figure 5b). Frequency shows a clear peak around the middle of the nineteenth century, indicating 10 of the most severe events occurred in this time period.

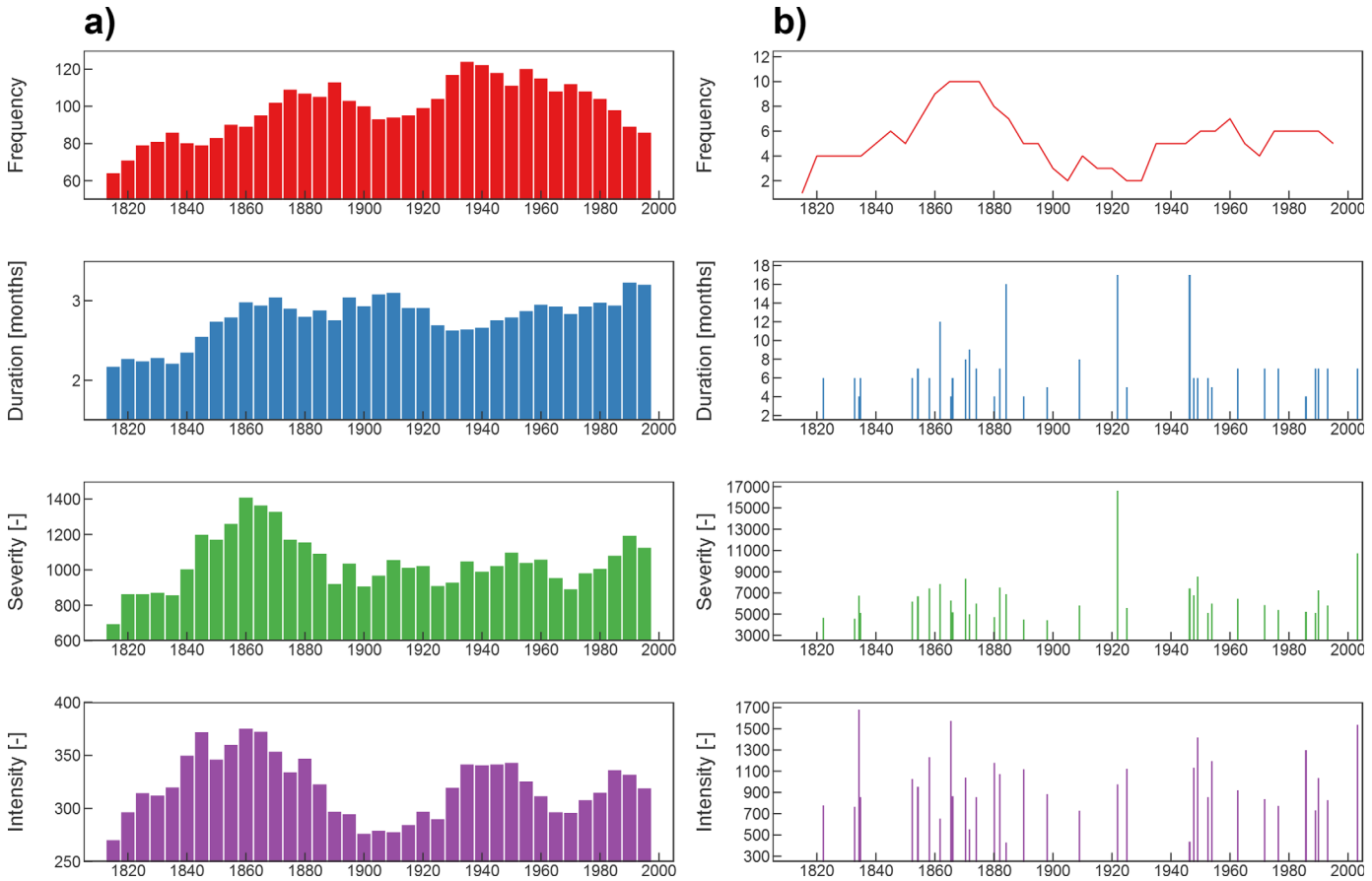

Figure 5. (column a) Frequency, duration, severity, and mean intensity (overlapping 30 year averages for duration, severity, and intensity and overlapping 30 year counts for frequency with a step of 5 years) of all identified drought events. (column b) The top 5% of the events (34 events) in terms of severity, where frequency is again the absolute count over 30 year windows with a step of 5 years, and duration, severity, and mean intensity are shown for the actual events.

On the other hand, the lowest frequencies are found from the end of the nineteenth century until the 1930s. Interestingly, the most severe event on record (October 1920 to February 1922, the 1921-event in Table 1) occurred right in that time period, suggesting that a large frequency does not necessarily imply the occurrence of very large events, and vice versa. In terms of drought duration there are only four of the most extreme drought events that lasted 1 year or longer, most of them show durations between 6 and 8 months. Only one of these three long-lasting droughts, the 1921-event, has high severities, which is due to the rather low intensities of the other two events.

Table 1
Top Ten Drought Events in the Greater Alpine Region Ranked by Severity

Rank	Period	Duration (months)	Peak	Severity	Mean intensity
1	Sep 1920 to Jan 1922	17	Oct 1921	16,610	977
2	Feb 2003 to Aug 2003	7	Mar 2003	10,742	1,534
3	Oct 1948 to Mar 1949	6	Jan 1949	8,513	1,418
4	Jan 1870 to Aug 1870	8	Apr 1870	8,322	1,040
5	Dec 1860 to Nov 1861	12	Sep 1861	7,819	652
6	Nov 1881 to May 1882	7	Dec 1881	7,517	1,074
7	Aug 1945 to Dec 1946	17	Apr 1946	7,442	438
8	Oct 1857 to Mar 1858	6	Jan 1858	7,403	1,234
9	Aug 1989 to Feb 1990	7	Nov 1989	7,258	1,037
10	May 1883 to Aug 1884	16	Feb 1884	6,856	429

The 1921-event is ranked #1 in terms of its severity (Table 1). The 2003-event is ranked #2; it gained its severity from the high mean intensity (1,534) rather than its duration (7 months). This is also the case for the 1948/1949-event on rank #3 with a mean intensity of 1,418, duration of 6 months and severity of 8,513. Out of the top 10 events, four last 12 months or longer and 6 events have durations between 6 and 8 months. Even though their severities may be similar, their other event characteristics may be very different, as illustrated by the events ranked #7 (1946-event, severity: 7,442) and #8 (1858-event, severity: 7,403), which have durations of 17 and 6 months, respectively, and mean intensities of 438 and 1,234, respectively. These dissimilarities suggest fundamental differences in the emergence of droughts which may be related to different manifestations of weather patterns and their persistence.

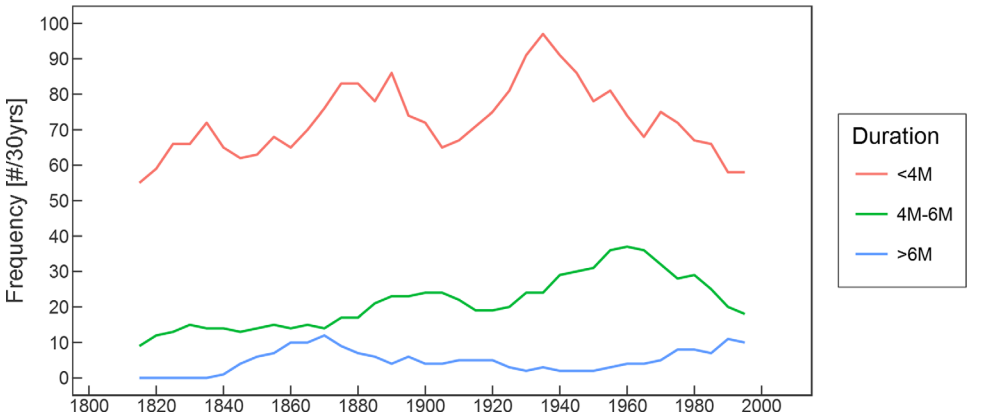

Figure 6. Thirty year running mean (5 year step) drought event frequency stratified by duration: short (<4 months), intermediate (4–6 months), and long (>6 months) events, based on all 663 events.

These results indicate that duration is a crucial drought feature. Indeed, Figure 6 shows a quite different evolution of drought frequency over time when stratifying the events into short (<4 months), intermediate (4–6 months), and long (>6 months) events. The frequency of short events is highest, clearly showing two peaks, one minor during the end of the nineteenth century and a major peak around the 1930s, indicating over 90 events per 30 years, with a subsequent decrease. Events with intermediate durations (4–6 months) show a constant increase in frequency peaking around the 1950s and 1960s, with a subsequent decrease. Long events occur more rarely and show a distinct peak around 1870, a flat minimum in the middle of the nineteenth century and a subsequent increase. There is therefore a shift from short/intermediate to long droughts in the past decades.

The seasonal behavior of the top 5% of the droughts is displayed in Figure 7. The monthly intensities (Figure 7a) highlight the absence of droughts in the first decades of the nineteenth as well as the twentieth century, whereas the rather wet beginning of the twentieth century was interrupted by the most severe 1921-event. The intensities averaged over 30 year periods (Figure 7b) shows highest values in winter and spring in the middle of the nineteenth century, peaking from 1851 to 1880 (late winter/early spring regime). In the following decades until the 1890s, winter months show increasing intensities, while the intensities in spring decrease (winter regime). During the first 40 years of the twentieth century, the relatively low extreme drought frequency is apparent, apart from the 1921-event and two cold-season events. From the 1940s, a general increase in intensity all year round is visible, but since the 1950s, autumn events (peaking in September) have become more frequent changing into a late summer/early autumn regime from 1961 to 1990.

4.2. Spatial Patterns

The spatial patterns of the detected drought events are assessed by the ratio of the number of times a grid point is considered as a DCR and the number of all events. For example, a ratio of 0.10 at a given grid point indicates that 10% of the whole number of events this grid point is part of a DCR. Figure 8a shows these fractions as maps for every grid point using all 663 detected events. There is a tendency for DCR to occur in northern Italy, particularly the Po-Plain (fraction of up to 0.10) and the French Rivera as well as in southern Hungary and parts of the Balkans. If one considers only the top 5% events in terms of severity, a different picture emerges (Figure 8b), and DCRs are more clearly separated and emerge predominantly in the Northwest of the domain as well as in the East. In both centers of mass of these two DCR hotspots, the fraction goes up to nearly 0.5, which means that during half the events these grid points are part of a DCR. The blue dashed line in Figures 8a and 8b indicates the approximate borders between the different drought regions by visual inspection. These are in line with the Alpine crest being a major climate divide in Europe. Subsequently, these subregions are referred to according to their location: Northwest, Southwest, and East.

DCRs rarely occur solely within one of these three subregions. More often they cross borders of the region boundaries, although Figure 8b clearly shows a Northwest and East concentration of DCRs. Thus, as a next step, the fraction of DCRs covering the subregions is determined and plotted for the top 5% events in Figure

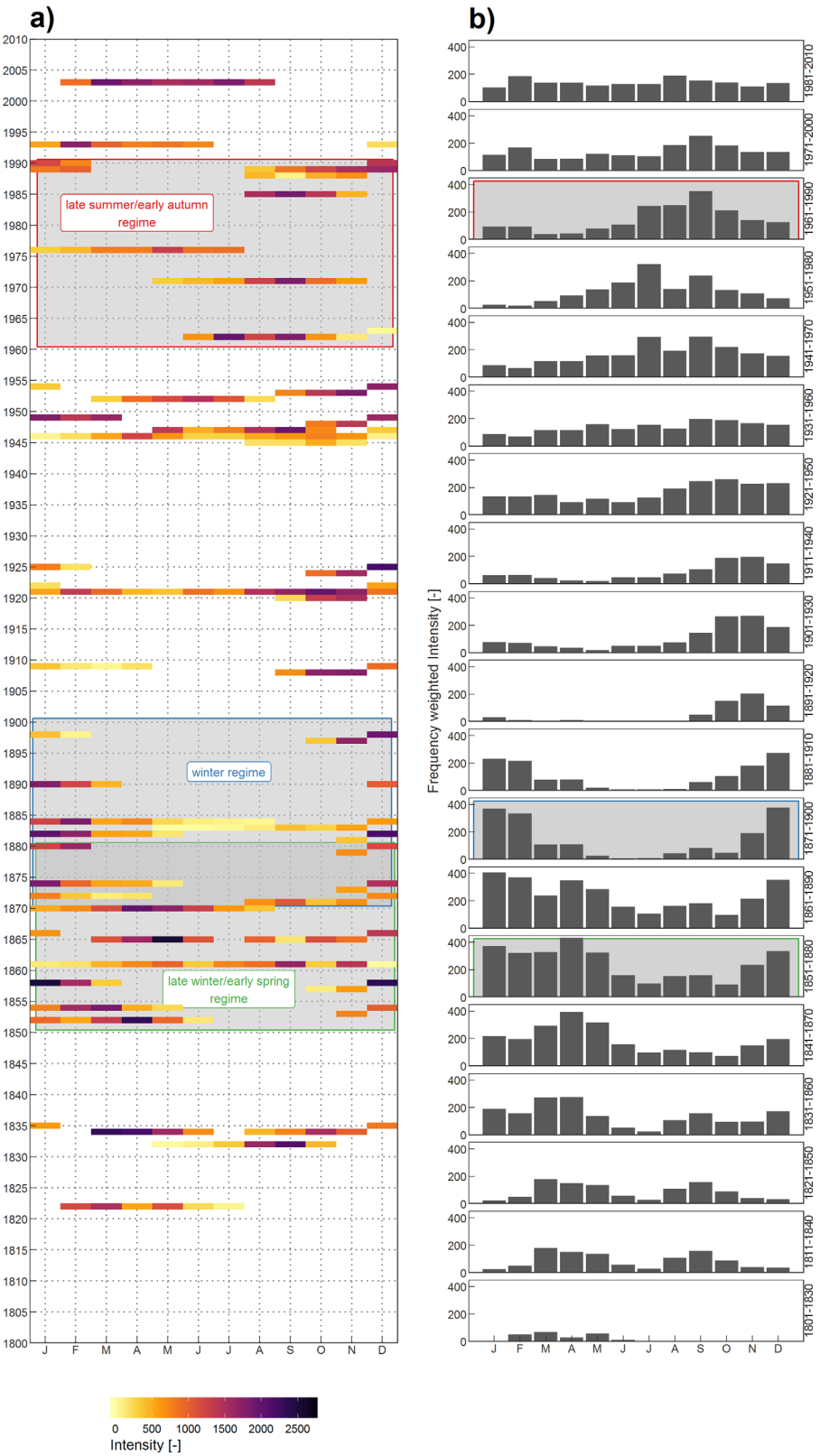

Figure 7. (a) Time of occurrence of the top 5% events in terms of their severity, colors indicate intensity of a given time step, horizontal axis is month, vertical axis is year. (b) Frequency-weighted monthly intensities in 30 year periods calculated for steps of 10 years; grey boxes indicate subperiods with strong seasonal regime differences.

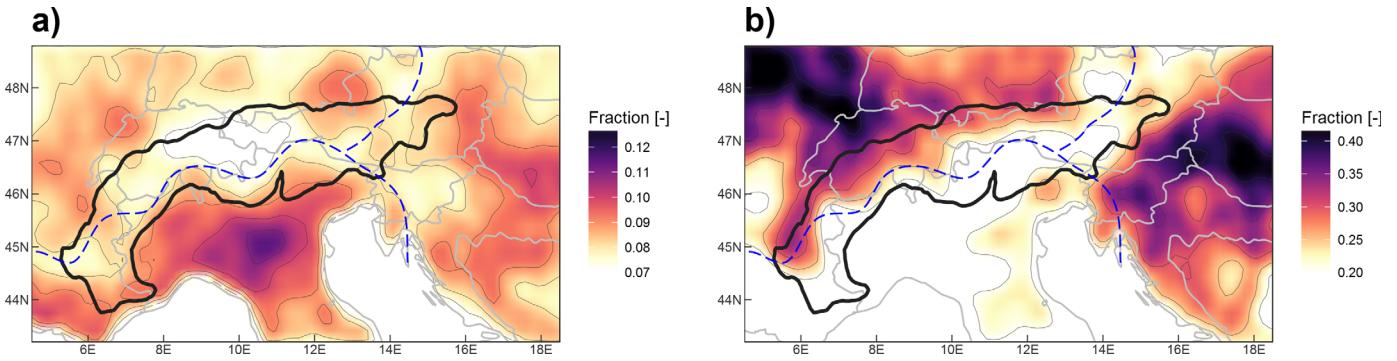

Figure 8. (a) Spatial patterns of DCRs for all events and (b) the top 5% events in terms of severity. The color shading indicates the fraction value which relates the number of times a grid point is part of a DCR relative to the total number of events considered (for Figure 8a: all events (663), for Figure 8b, top 5% (34)). The higher the fraction (darker color), the more often a grid point is part of a DCR. The dashed blue line indicates approximate borders of drought regions.

9. Most DCRs cannot be attributed to one single region, but there are preferred regions. The fraction of DCRs covering the Southwest region tends to be smaller than those of the other two. This is consistent with Figure 8b where the rather low fractions are given in the Southwest considering the most extreme events.

The drought-intense time period around the middle to the late nineteenth century mostly consists of events with DCRs predominantly covering the Northwest (seven events), with only two events contributing mainly to the Southwest and East. Typically, Northwest occurrence is also apparent during the few events in the first decades of the twentieth century. However, in the period from 1940 to 1950, with increased extreme event frequency, DCRs move toward the East, where all events show the highest fraction of DCR coverage.

In the light of this spatial analysis, the previously described seasonal shift of extremes from winter/spring (end of nineteenth century) toward autumn (end of twentieth century) has to be considered as a shift in space as well as a shift in seasonality, implying a fundamental feature of drought occurrence in the GAR. This could be due to changes in the mid latitude circulation since the end of the Little Ice Age as indicated by Schwander et al. (2017). They found increased frequencies of high pressure patterns over Central Europe from 1960 onward, which could explain the dominance of Eastern droughts in that period, and increased frequencies of Northern Cyclonic patterns and Westerly flow over Southern Europe patterns during the period from 1850 to 1880, which may be related to the droughts predominantly affecting the Northwest.

Figure 10 shows the DCR fractions for events considering different durations, independent of the severity. Short-term events (Figure 10a) are most abundant which explains the similarity with Figure 8a. As can be seen in Figure 10b, the spatial patterns of intermediate events (148 events) show their DCRs mostly in the North and East of the domain, and the long events (Figure 10c, 34 events) show the preferred location in the Northwest and the East.

4.3. The Drought-Temperature Nexus

The large sample of droughts over the last two centuries offers the opportunity to assess the long-term relationship between air temperatures and drought characteristics. In the GAR, air temperatures in the period

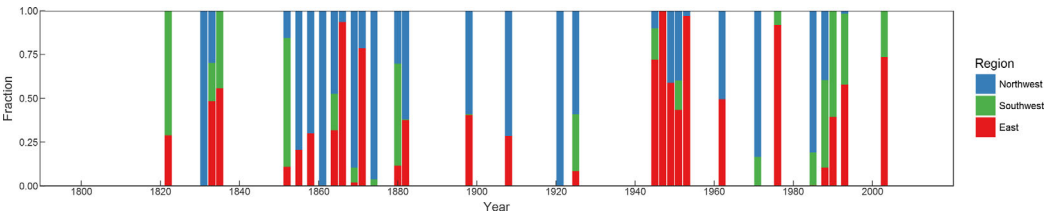

Figure 9. Fraction of DCRs covering subregions. Vertical bars indicate the time of occurrence of the top 5% events by severity. The color of the bars indicates the fractional overlap over subregions. The horizontal positions of the bars have been slightly adjusted for them to plot without overlap.

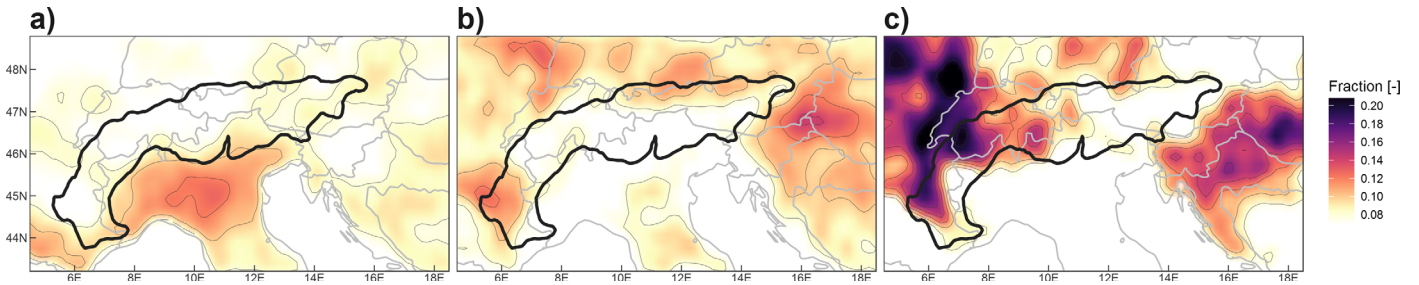

Figure 10. Spatial patterns of DCRs for short events (a, duration < 4 months), intermediate events (b, duration 4–6 months), and long events (c, duration > 6 months). The color shading indicates the fraction value which relates the number of times a grid point is part of a DCR relative to the whole number of events considered (for Figure 10a: short events (481), for Figure 10b, intermediate events (148), for Figure 10c, long events (34)). The higher the fraction (darker color) the more often a grid point is part of a DCR.

1900–2000 have increased, on average, by 1.2°C based on linear trend analysis (Auer et al., 2007). We calculated annual average air temperatures over the whole domain of the GAR and identified the coolest and warmest 30 year period, which turned out to be 1876–1905 and 1981–2010, respectively. The corresponding temperatures are 7.86 and 9.27°C, respectively (Table 2). The difference thus is 1.41°C, which is slightly above the nineteenth century temperature change of Auer et al. (2007) as mentioned above. The average drought characteristics (duration, mean intensity, severity, and 30 year frequency) of the coolest and the warmest periods are given in Table 2. Duration shows an increase from the cool to the warm period from 2.75 to 3.20 months which is consistent with Figure 6. Mean intensity increased from 297 to 319, and severity from 921 to 1125, although these changes are not significant. However, frequency decreased from 113 to 86 detected events. These results suggest that the recent warming climate has, so far, not significantly affected the drought characteristics in the GAR.

The seasonal aspects of the drought-temperature nexus are displayed in Figure 11. Each event emerging in the three winter months (DJF) and the three summer months (JJA) is shown as a circle (having events with durations > 3 months only these three seasonal months are extracted); drought intensity during these 3 months is indicated by the size of the circle, and vertical position and color indicate the associated temperature anomaly of this event.

In winter (Figure 11a), droughts with both positive and negative temperature anomalies occur. This behavior is related to air temperatures in winter mainly being forced by the advected air masses in the GAR, either cold or warm, dependent on the large scale circulation characteristics (Auer et al., 2007). This is not only true of the overall temperature characteristics but also of those during droughts. Really cold winter droughts with temperature anomalies below −3°C occurred mostly in the late nineteenth century and the first half of the twentieth century. From the 1950s onward, there is an absence of such events. Running correlation of mean intensity and temperature anomaly (30 year window, Figure 11c) reveals no relationship until the 1970s, however, afterward a steep increase in correlation is apparent, indicating higher mean intensities associated with higher temperature anomalies in the recent past.

Table 2
Mean Temperature, Duration, Mean Intensity, Severity, and Frequency of Drought Events in the Coolest and Warmest 30 Year Periods in the GAR

	Coolest period 1876–1905	Warmest period 1981–2010	*p*-value
Temperature (°C)	7.86	9.27	0.00**
Duration (months)	2.75	3.20	0.10
Mean intensity	297	319	0.66
Severity	921	1,125	0.24
Frequency (#/30 years)	113	86	

Note. Significance of the difference between the two periods expressed by the *p*-value of the Wilcoxon test statistic.
**Significance at the 5% level ($p < 0.05$).

Summer temperatures (Figure 11b) show a smaller year to year variability, and droughts are more likely associated with above average temperatures. This would be expected as the absence of rainfall is usually accompanied by lack of clouds, high sunshine duration and therefore higher temperatures. However, there is no clear indication that high positive temperatures are also associated with high intensities, although the 2003-event stands out as a single event where this is the case (Wetter et al., 2014). Interestingly, the 2003-event was not the most intense summer drought, it was the summer of 1962 which was even drier than 2003, although its temperature anomaly was slightly below average (–0.4°C). This suggests that dry summers are not necessarily hot. Additional analyses (not shown) indicate, that the circulation patterns during these two summers were rather different; in 2003 a blocked weather situation governed the drought with

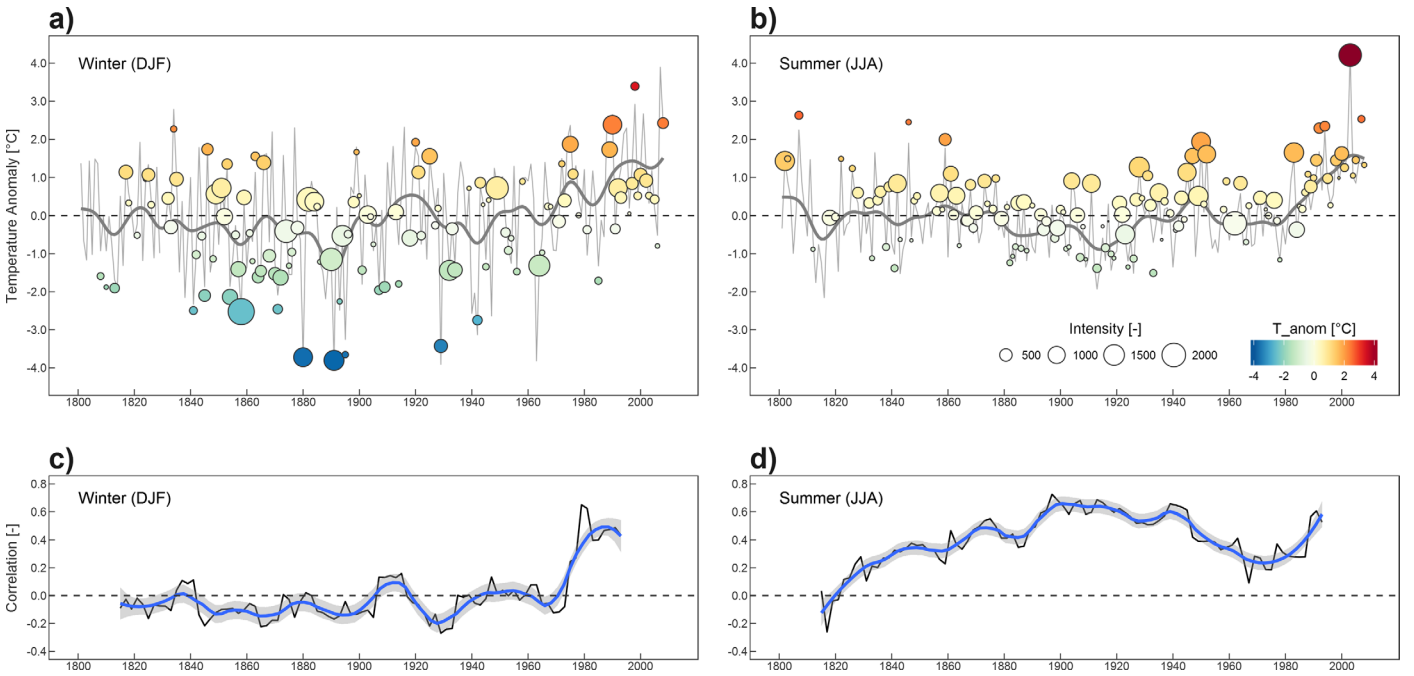

Figure 11. (top) Mean intensities and corresponding temperature anomalies of drought events of a minimum duration of 3 months covering (a) winter (DJF) and (b) summer (JJA). Size of circles indicates intensity; location along the vertical axis and the color shading indicate temperature anomaly. In the background, the seasonal mean temperature anomalies of the whole GAR are plotted in grey (thin line: seasonal means, thick line: 20 year Gaussian filtered seasonal means). (bottom) Running correlation (Spearman rank correlation) of mean intensity and temperature anomaly over 30 year periods with a step of 2 years.

increased subtropical warm air advection, while in 1962 westerly (cool) airflow from the Atlantic into the GAR dominated. However, the running correlation analysis (Figure 11d) shows an increase from zero at the beginning of the nineteenth century up to 0.6 around the late nineteenth/early twentieth century, and a decrease afterward until the 1970s, followed again by an increase in correlation. These results suggest that the positive relationship between mean intensity and temperature anomaly is stronger during periods with cooler climate conditions, as summers tended to be coolest at the beginning of the twentieth century.

The drought-temperature relationship is further analyzed in Figure 12 which shows the drought intensity and temperature anomaly for the two periods from Table 2, stratified by season similar to Figure 10. During cool climate conditions (1876–1905), some major winter events had very low temperatures while the summer events show smaller temperature anomalies compared to the long-term mean. As mentioned earlier, events with high mean intensity and considerable negative temperature anomalies did not occur in recent decades. In the cool decades at the end of the nineteenth century, high mean intensities are apparent for very cold, as well as for slightly above temperature anomalies, indicating a large spread of temperature characteristics during droughts, which is consistent with the running correlation analysis of Figure 11c. All these findings point toward major changes in the weather patterns leading to droughts, particularly the location of precipitation-inhibiting high pressure systems and the associated air mass advection into the GAR. During warm climate conditions (1981–2010), the summer events, again, show smaller temperature anomalies if one does not count the 2003-event which has been extraordinary. It is interesting that the cold period featured two cold outliers while the warm period featured a warm outlier.

The distribution properties of the mean intensity on a seasonal basis are evaluated by Empirical Cumulative Distribution Functions (ECDFs) of the mean intensity stratified by temperature anomalies (Figure 13). In winter (DJF), higher drought intensities are associated with near normal or below average temperatures. The less pronounced tail of the intensity distribution for the warm events indicates less potential for warm winter droughts with high intensities. Cold winter droughts are likely to be caused by continental high pressure systems which tend to be very persistent, which may not be the case for the warm winter droughts. In spring (MAM), no clear shift in the intensity distribution of different temperature stratifications is apparent. However, in summer (JJA), rather different ECDFs are apparent, indicating that higher drought intensities

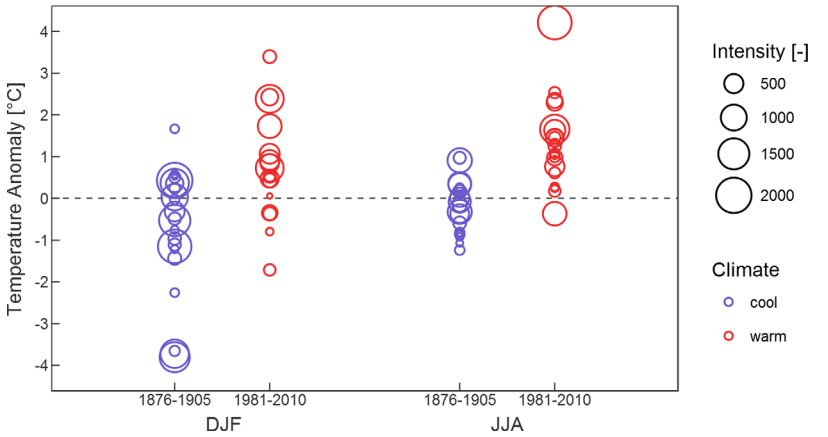

Figure 12. Intensity and respective temperature anomaly of drought events of a minimum duration of 3 months covering winter (DJF) and summer (JJA), during 30 year periods of coolest/warmest climate conditions (cool: 1876–1905, warm: 1981–2010).

are associated with higher temperature anomalies and, conversely, cool summer droughts are usually not very intense. The same signal is apparent in autumn (SON) but is less distinctive.

While intense summer droughts (such as the 2003-event, see Figure 10b) tend to be warmer than average, this was not the case for the 1962-event. The two events also differed in terms of their temporal evolution. The 2003-event started in February (see Figure 7a), whereas the 1962-event started in June with normal precipitation conditions during spring. This suggests that the summer temperature anomaly during droughts may be related to preceding spring precipitation. We therefore analyzed summer droughts and separated those with dry springs from those where the drought did not start before summer. The Probability Density Functions of the monthly temperature anomalies from May to August for both samples are plotted in Figure 14. A distinct shift toward higher temperature anomalies during summer with dry spring preconditions (mean temperature anomaly: +0.73°C) is apparent compared to those events where spring was wet (mean temperature anomaly: +0.30°C). This difference in the mean is significant according to the Wilcoxon test on the 5% level (*p*-value: 0.042). Also noticeable is a broader right tail of the distribution (positive temperature anomalies).

5. Discussion

In this paper, we present a new method for identifying meteorological drought events based on connected space-time regions. We analyze a 210 year precipitation data set to explore drought event durations, intensities, severities, and frequencies. As would be expected, well-known severe droughts rank highly in the results, such as the 2003-event (Fink et al., 2004; Wetter et al., 2014), the 1921-event (Brooks & Glasspoole, 1922), and the 1946-event (Brázdil et al., 2016).

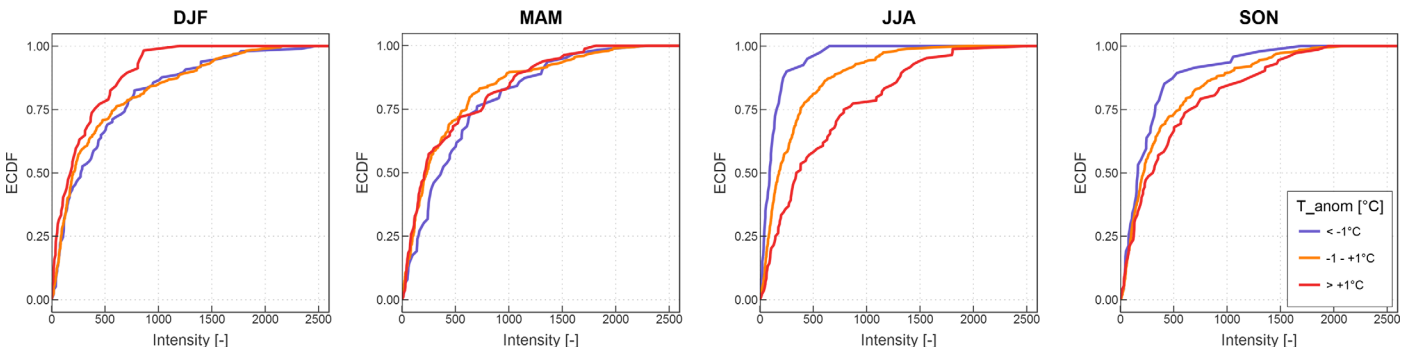

Figure 13. Empirical Cumulative Distribution Functions of drought Intensities (over 3 months) stratified by seasons: winter, DJF; spring, MAM; summer, JJA; and autumn, SON, and stratified by the corresponding temperature anomaly; below average, blue; near average, yellow; above average, red.

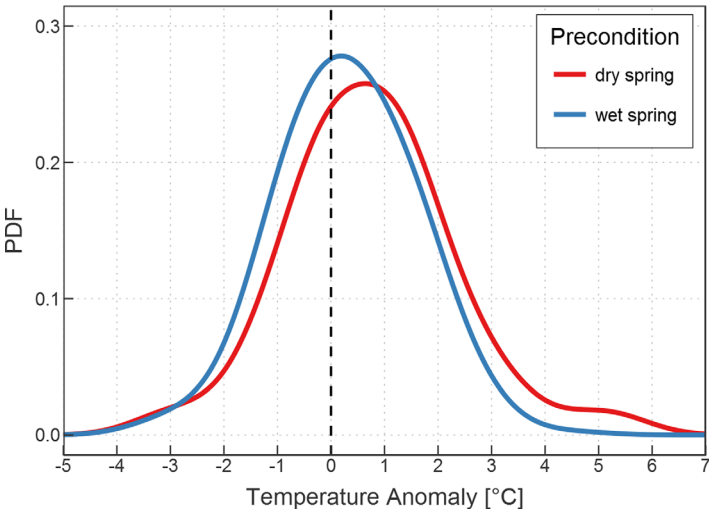

Figure 14. Probability Density Function (PDF) of monthly temperature anomalies during May–August, stratified by drought conditions of the preceding spring. Red, drought event covering spring and summer (dry spring precondition); blue, drought event covering only summer (wet spring precondition).

Our results on the temporal evolution of droughts during the last two centuries is in close agreement with previous studies that have tagged the 1940s and the period from 1850 to 1880 (the 1860s period) as drought prone time periods (e.g., Lloyd-Hughes, 2012; Lloyd-Hughes & Saunders, 2002; van der Schrier et al., 2007). Here we were able to clearly distinguish these two periods from their spatio-temporal features. The 1860s period shows the highest values in both severity and mean intensity as well as in frequency of the major (top 5%) droughts. At the same time, the analysis of frequency stratified by duration revealed that this period shows a peak in the occurrence of long (>6 months) droughts. In contrast, the 1940s show only slightly lower mean intensities, but severity is not peaking. This is related to the low frequency of long droughts, while short (<4 months) and intermediate (4–6 months) events show rather high frequencies.

The seasonal patterns exhibited a major shift of the extreme droughts from a winter/spring dominated regime in the 1860s toward an autumn regime in the 1960s, whereas the period around the 1940s shows no strong seasonality. A possible mechanism of the 1940s droughts could be the expansion of the tropical belt and the Hadley cell during that time period (Brönnimann et al., 2015) which may have caused more subtropical high pressure systems to affect Central Europe. This would also be consistent with the joint drought/temperature assessment showing a clear peak in the intensity and temperature anomaly of summer droughts in the 1940s (see Figure 10). However, this is not consistent with the results of Schwander et al. (2017) who showed that high pressure weather patterns over Europe did not peak during this period. Their results indicate weather patterns with easterly or northerly flow to dominate.

Whereas in the 1940s, it was predominantly the East of the domain which was most affected by droughts, in the 1860s it was the Northwest. While the reasons for these differences are not fully clear due to data limitations, the features of the 1860s with their highest mean intensities, long durations, and winter/spring dominance point toward high frequency and/or high persistency of high pressure weather patterns over Central Europe which might be introduced by a wavier jet stream bearing the potential for excessive blocking situations. We also found a transition in seasonality from the 1860s (high winter/spring intensities) toward the end of the twentieth century (higher autumn intensities). Interestingly, this seasonal shift is accompanied by a spatial change from the Northwest to the Southeast. The location of drought centers is primarily driven by the location of the drought inducing weather patterns (e.g., high pressure systems). Schwander et al. (2017) found higher frequencies of high pressure systems over Central Europe from the 1960s to the 1990s, which would confirm the higher drought intensities in that period. In contrast, no such peak is apparent during the middle of the nineteenth century, the period with the highest drought intensities. Above average high pressure situations are therefore not likely the main cause. It is possible that the location of the high pressure pattern does not have to be over Central Europe, given that the Northwest is the area most affected by droughts during this period. Extensive highs over the British Isles could also affect the Northwestern GAR and would be accompanied with northerly airflow. Increased frequencies of weather patterns with Northerly airflow have been found by Schwander et al. (2017) during the 1860s and could explain the frequent high intensity droughts in the Northwestern GAR. There is, however, room for better understanding the atmospheric drivers in this period.

The evaluation of the temperature increase in the GAR in relation to drought characteristics yielded no significant relationships, although previous studies (Dai, 2011; van der Schrier et al., 2006, 2007) did report increasing drought conditions over Central Europe during recent decades. This is mainly due to fact that drought indices, such as the PDSI where a temperature based parameterization of evapotranspiration is used, imply a relationship between droughts and temperature. Trends of changing weather patterns in the mid-latitudes over the last decades (Weusthoff, 2011) point toward an increased frequency of high pressure weather patterns over Central Europe, but this does not seem to manifest itself in more severe or frequent droughts. We did find a significant shift in the temperature anomalies during summer droughts dependent on the spring preconditions (wet/dry). Mueller and Seneviratne (2012) identified a positive relationship

between preceding negative SPI values and the occurrence for hot days in Europe and other parts of the world. These and our findings suggest that soil moisture-temperature coupling is of major importance for drought development in the warm season, as it could increase drought stress through enforced evapotranspiration. Although there is no clear signal of increased summer drought intensity or frequency apparent from the precipitation analysis in this paper, further increasing trends of high pressure pattern frequency over Europe in winter and spring (Weusthoff, 2011) may have implications on summer droughts in a warming climate.

The new method of drought detection proposed in this paper allowed for an objective analysis of drought characteristics, including drought duration. However, the method does have its limitations. It is based on a connectivity approach where connected space-time elements of below threshold precipitation are connected to a coherent region, i.e., the space-time drought event. While the connectivity approach is attractive as it is able to identify events, rather than minima of an index, it is not fully independent of the space and time resolution used in the analysis (see Western et al., 1998, 2001 for a discussion of grid resolution in the context of soil moisture connectivity). The smaller the space-time discretization, the smaller tend to be the regions identified, as a coarser resolution averages out any small scale features that may interrupt a coherent space-time region. We used a 3 month temporal averaging and a spatial resolution of 10 arc min ($\sim$16 km). It would be interesting to analyze the effect of the resolution on the results. Preliminary analyses suggest that there is an effect on the absolute value of the drought characteristics, but the space-time patterns of the results (long-term variability, spatial patterns of drought core regions) change very little. Future work could be directed toward more quantitatively analyzing the atmospheric drivers of the space-time drought patterns, both in Europe and elsewhere. Finally, the method could be readily applied to drought realms other than meteorological droughts (agricultural, hydrological droughts) by using soil moisture and streamflow in addition to existing pooling methods for obtaining temporally coherent hydrological drought events (e.g., Laaha et al., 2017).

6. Conclusion

In this paper, we proposed a new method for detecting atmospheric drought events and their space-time structure. We used the method to analyze the long-term evolution of drought frequency, duration, intensity, and severity over the past 210 years in the Greater Alpine Region (GAR) in Central Europe. Our results show variations of these characteristics on multidecadal time scales, but no trends over the 210 year period are apparent. Two periods (the 1860s and 1940s) stand out as drought periods, although the characteristics of individual droughts in these decades are substantially different, indicating different driving mechanisms. The most extreme droughts show their centers either in the Northwest or the Southeast of the GAR, with a larger number of Northwest events in the nineteenth century and a shift toward Southeast events in the second half of the twentieth century. Although temperatures increased significantly during the period, we did not find the increase to be significantly correlated with drought duration, intensity, or severity. However, we found that dry springs significantly increase temperatures during subsequent summer droughts, which implies soil moisture-temperature coupling in the warm season. Further research should be directed toward better understanding the drivers of long-term drought fluctuations.

Acknowledgments
K. Haslinger is a recipient of a DOC fellowship (24147) of the Austrian Academy of Sciences which is gratefully acknowledged for financial support. Funding from the Austrian Science Foundation as part of the Vienna Doctoral Programme on Water Resource Systems (DK Plus W1219-N22) is acknowledged. The authors also thank the Climate Research Unit of the University of East Anglia for hosting the Greater Alpine Region precipitation data set and the Central Institute for Meteorology and Geodynamics for providing the HISTALP temperature data set. The paper is a contribution to UNESCO's FRIEND-Water program. The authors thank two reviewers for their valuable comments on the manuscript.

References

Andreadis, K. M., Clark, E. A., Wood, A. W., Hamlet, A. F., & Lettermaier, D. P. (2005). Twentieth-century drought in the conterminous United States. *Journal of Hydrometeorology*, *6*(6), 985–1001. https://doi.org/10.1175/JHM450.1

Auer, I., Böhm, R., Jurkovic, A., Lipa, W., Orlik, A., Potzmann, R., . . . Nieplova, E. (2007). HISTALP—Historical instrumental climatological surface time series of the Greater Alpine Region. *International Journal of Climatology*, *27*, 17–46. https://doi.org/10.1002/joc.1377

Beniston, M. (2009). Trends in joint quantiles of temperature and precipitation in Europe since 1901 and projected for 2100. *Geophysical Research Letters*, *36*, L07707. https://doi.org/10.1029/2008GL037119

Brázdil, R., Raška, P., Trnka, M., Zahradní, P., Valášek, H., Dobrovolný, P., . . . Stachon, Z. (2016). The Central European drought of 1947: Causes and consequences, with particular reference to the Czech Lands. *Climate Research*, *70*, 161–178. https://doi.org/10.3354/cr01387

Brönnimann, S., Fischer, A. M., Rozanov, E., Poli, P., Compo, G. P., & Sardeshmukh, P. D. (2015). Southward shift of the northern tropical belt from 1945 to 1980. *Nature Geoscience*, *8*, 969–974. https://doi.org/10.1038/ngeo2568

Brooks, C. E. P., & Glasspoole, J. (1922). The drought of 1921. *Quarterly Journal of the Royal Meteorological Society*, *48*(202), 139–168. https://doi.org/10.1002/qj.49704820205

Burke, E. J., & Brown, S. J. (2008). Evaluating uncertainties in the projection of future drought. *Journal of Hydrometeorology*, *9*, 292–299. https://doi.org/10.1175/2007JHM929.1

Chimani, B., Matulla, C., Böhm, R., & Hofstätter, M. (2013). A new high resolution absolute temperature grid for the Greater Alpine Region back to 1780. *International Journal of Climatology*, *33*(9), 2129–2141. https://doi.org/10.1002/joc.3574

Dai, A. (2011). Characteristics and trends in various forms of the Palmer Drought Severity Index during 1900–2008. *Journal of Geophysical Research*, *116*, D12115. https://doi.org/10.1029/2010JD015541

Dai, A., Trenberth, K. E., & Qian, T. (2004). A global dataset of Palmer Drought Severity Index for 1870–2002: Relationship with soil moisture and effects of surface warming. *Journal of Hydrometeorology*, *5*(6), 1117–1130. https://doi.org/10.1175/JHM-386.1

Efthymiadis, D., Jones, P. D., Briffa, K. R., Auer, I., Böhm, R., Schöner, W., . . . Schmidli, J. (2006). Construction of a 10-min-gridded precipitation data set for the Greater Alpine Region for 1800–2003. *Journal of Geophysical Research*, *111*, D01105. https://doi.org/10.1029/2005JD006120

Fink, A. H., Brücher, T., Krüger, A., Leckebusch, G. C., Pinto, J. G., & Ulbrich, U. (2004). The 2003 European summer heatwaves and drought—Synoptic diagnosis and impacts. *Weather*, *59*(8), 209–216. https://doi.org/10.1256/wea.73.04

García-Herrera, R., Díaz, J., Trigo, R. M., Luterbacher, J., & Fischer, E. M. (2010). A review of the European Summer Heat Wave of 2003. *Critical Reviews in Environmental Science and Technology*, *40*, 267–306. https://doi.org/10.1080/10643380802238137

IPCC. (2012). In C. B. Field et al. (Eds.), *Managing the risks of extreme events and disasters to advance climate change adaptation. A special report of Working Groups I and II of the Intergovernmental Panel on Climate Change* (582 pp.). Cambridge, UK: Cambridge University Press.

Kendon, M., Marsh, T., & Parry, S. (2013). The 2010–2012 drought in England and Wales. *Weather*, *68*(4), 88–95. https://doi.org/10.1002/wea.2101

Laaha, G., Gauster, T., Tallaksen, L. M., Vidal, J.-P., Stahl, K., Prudhomme, C., . . . Wong, W. K. (2017). The European 2015 drought from a hydrological perspective. *Hydrology and Earth System Sciences*, *21*(6), 3001–3024. https://doi.org/10.5194/hess-21-3001-2017

Lloyd-Hughes, B. (2012). A spatio-temporal structure-based approach to drought characterization. *International Journal of Climatology*, *32*, 406–418. https://doi.org/10.1002/joc.2280

Lloyd-Hughes, B., & Saunders, M. A. (2002). A drought climatology for Europe. *International Journal of Climatology*, *22*, 1571–1592. https://doi.org/10.1002/joc.846

McKee, T. B., Doeskin, N. J., & Kleis, J. (1993). The relationship of drought frequency and duration to time scales (Preprints). In *8th conference on applied climatology* (pp. 179–184). Boston, MA: American Meteorological Society.

Mishra, A. K., & Singh, V. P. (2010). A review of drought concepts. *Journal of Hydrology*, *391*(1–2), 202–216. https://doi.org/10.1016/j.jhydrol.2010.07.012

Mueller, B., & Seneviratne, S. I. (2012). Hot days induced by precipitation deficits at the global scale. *Proceedings of the National Academy of Sciences of the United States of America*, *109*(31), 12398–12403. https://doi.org/10.1073/pnas.1204330109

Naresh Kumar, M., Murthy, C. S., Sesha Sai, M. V. R., & Roy, P. S. (2009). On the use of Standardized Precipitation Index (SPI) for drought intensity assessment. *Meteorological Applications*, *16*, 381–389. https://doi.org/10.1002/met.136

Palmer, W. C. (1965). *Meteorological drought* (Tech. Rep. Weather Bur. Res. Pap. 45). Washington, DC: U.S. Department of Commerce.

Patel, N. R., Chopa, P., & Dadhwal, V. K. (2007). Analyzing spatial patterns of meteorological drought using Standardized Precipitation Index. *Meteorological Applications*, *14*, 329–336. https://doi.org/10.1002/met.33

Samaniego, L., Kumar, R., & Zink, M. (2013). Implications of parameter uncertainty on soil moisture drought analysis in Germany. *Journal of Hydrometeorology*, *14*, 47–68. https://doi.org/10.1175/JHM-D-12-075.1

Schwander, M., Brönnimann, S., Delaygue, G., Rohrer, M., Auchmann, R., & Brugnara, Y. (2017). Reconstruction of Central European daily weather types back to 1763. *International Journal of Climatology*, *37*, 30–44. https://doi.org/10.1002/joc.4974

Seneviratne, S. I., Lüthi, D., Litschi, M., & Schär, C. (2006). Land–atmosphere coupling and climate change in Europe. *Nature*, *443*, 205–209. https://doi.org/10.1038/nature05095

Sheffield, J., Andreadis, K. M., Wood, E. F., & Lettenmaier, D. P. (2009). Global and continental drought in the second half of the twentieth century: Severity-Area-Duration analysis and temporal variability of large-scale events. *Journal of Climate*, *22*(8), 1962–1981. https://doi.org/10.1175/2008JCLI2722.1

Sheffield, J., & Wood, E. F. (2007). Characteristics of global and regional drought, 1950–2000: Analysis of soil moisture data from off-line simulation of the terrestrial hydrologic cycle. *Journal of Geophysical Research*, *112*, D17115. https://doi.org/10.1029/2006JD008288

Sheffield, J., & Wood, E. F. (2008). Global trends and variability in soil moisture and drought characteristics, 1950–2000, from observation-driven simulations of the terrestrial hydrologic cycle. *Journal of Climate*, *21*, 432–458. https://doi.org/10.1175/2007JCLI1822.1

Spinoni, J., Naumann, G., Vogt, J. V., & Barbosa, P. (2015). The biggest drought events in Europe from 1950 to 2012. *Journal of Hydrology: Regional Studies*, *3*, 509–524. https://doi.org/10.1016/j.ejrh.2015.01.001

Stagge, J. H., Tallaksen, L. M., Gudmunsson, L., van Loon, A. F., & Stahl, K. (2015). Candidate distributions for climatological drought indices (SPI and SPEI). *International Journal of Climatology*, *35*, 4027–4040. https://doi.org/10.1002/joc.4267

Svoboda, M., Lecomte, D., Hayes, M., Heim, R., Gleason, K., Angel, J., . . . Stephens, S. (2002). The drought monitor. *Bulletin of the American Meteorological Society*, *83*(8), 1181–1190.

UNEP. (2006). Impacts of summer 2003 heat wave in Europe. *Environmental Alert Bulletin*, Nairobi, Kenya.

Van den Dool, H. M., Saha, S., & Johansson, A. (2000). Empirical Orthogonal Teleconnections. *Journal of Climate*, *13*(8), 1421–1435. https://doi.org/10.1175/1520-0442(2000)013<1421:EOT>2.0.CO;2

van der Schrier, G., Briffa, K. R., Jones, P. D., & Osborne, T. J. (2006). Summer moisture variability across Europe. *Journal of Climate*, *19*, 2818–2834. https://doi.org/10.1175/JCLI3734.1

van der Schrier, G., Efthymiadis, D., Briffa, K. R., & Jones, P. D. (2007). European Alpine moisture variability for 1800–2003. *International Journal of Climatology*, *27*, 415–427. https://doi.org/10.1002/joc.1411

van der Schrier, G., Barichivich, J., Briffa, K. R., & Jones, P. D. (2013). A scPDSI-based global data set of dry and wet spells for 1901–2009. *Journal Geophysical Research: Atmosphere*, *118*, 4025–4048. https://doi.org/10.1002/jgrd.50355

van Lanen, H. A. J., Laaha, G., Kingston, D. G., Gauster, T., Ionita, M., Vidal, J. P., . . . van Loon, A. F. (2016). Hydrology needed to manage droughts: The 2015 European case. *Hydrological Processes*, *30*, 3097–3104. https://doi.org/10.1002/hyp.10838

Vincente-Serrano, S. M. (2006). Differences in spatial patterns of drought on different time scales: An Analysis of the Iberian Peninsula. *Water Resources Management*, *20*, 37–60. https://doi.org/10.1007/s11269-006-2974-8

Vincente-Serrano, S. M., Beguería, S., Lorenzo-Lacruz, J., Camarero, J. J., López-Moreno, J. I., Azorin-Molina, C., . . . Sanchez-Lorenzo, A. (2012). Performance of drought indices for ecological, agricultural and hydrological applications. *Earth Interactions*, *16*, 010. https://doi.org/10.1175/2012EI000434.1

Wells, N., Goddard, S., & Hayes, M. (2004). A self-calibrating Palmer Drought Severity Index. *Journal of Climate*, *17*, 2335–2351. https://doi.org/10.1175/1520-0442(2004)017<2335:ASPDSI>2.0.CO;2

Western, A. W., Blöschl, G., & Grayson, R. B. (1998). How well do indicator variograms capture the spatial connectivity of soil moisture? *Hydrological Processes*, *12*, 1851–1868. https://doi.org/10.1002/(SICI)1099-1085(19981015)12:12<1851::AID-HYP670>3.0.CO;2-P

Western, A. W., Blöschl, G., & Grayson, R. B. (2001). Towards capturing hydrologically significant connectivity in spatial patterns. *Water Resources Research*, *37*(1), 83–97. https://doi.org/10.1029/2000WR900241

Wetter, O., Pfister, C., Werner, J. P., Zorita, E., Wagner, S., Seneviratne, S. I., . . . Spring, J.-L. (2014). The year-long unprecedented European heat and drought of 1540—A worst case. *Climatic Change*, *125*(3), 349–363. https://doi.org/10.1007/s10584-014-1184-2

Weusthoff, T. (2011). Weather type classification at MeteoSwiss: Introduction of new automatic classification schemes. *Arbeitsberichte der MeteoSchweiz*, *235*, 46.

Zhai, J., Huang, J., Su, B., Cao, L., Wang, Y., Jiang, T., & Fischer, T. (2017). Intensity–area–duration analysis of droughts in China 1960–2013. *Climate Dynamics*, *48*(1–2), 151–168. https://doi.org/10.1007/s00382-016-3066-y